

Received 23 June 2024, accepted 10 July 2024, date of publication 15 July 2024, date of current version 24 July 2024.

Digital Object Identifier 10.1109/ACCESS.2024.3427793

RESEARCH ARTICLE

Enhancing MEC Offloading Performance With NOMA-CDRT in the Presence of Impaired Hardware

SUDHIR KUMAR SA^{ID} AND ANOOP KUMAR MISHRA^{ID}, (Member, IEEE)

School of Electronics Engineering, VIT-AP University, Amaravati, Andhra Pradesh 522237, India

Corresponding author: Anoop Kumar Mishra (anoop1mishra@gmail.com)

This work was supported by Vellore Institute of Technology-Andhra Pradesh (VIT-AP) University.

ABSTRACT Recently, mobile edge computing (MEC) has been proposed to improve wireless devices' computational capabilities by offloading computation-intensive tasks to a network-edge server. Analytical research indicates that the application of non-orthogonal multiple access (NOMA) can significantly reduce the latency and energy consumption of MEC offloading. In order to capture the potential gains of NOMA in the context of MEC, this paper proposes an edge computing-aware coordinated direct and relay transmission (CDRT) based NOMA technique which can enjoy the benefits of uplink NOMA in reducing MEC users' uplink energy consumption and computational delay. By lowering the likelihood of uplink outages for MEC users, the NOMA-assisted MEC system can benefit from uplink NOMA's advantages. In addition, CDRT-based NOMA has the sum capacity scaling of $\log \rho_b$ as signal-to-noise-ratio ρ_b increases, but $\frac{1}{2} \log \rho_b$ for non-CDRT-based NOMA. Hence, applying CDRT-based NOMA in MEC increases the computation capability and decreases communication outage probability by extending the cell coverage of the MEC users. Based on this idea and the superior performance requirements in future wireless networks, we derive new closed-form expressions for the exact ergodic sum capacity and offloading outage probability under both residual hardware impairment and perfect/imperfect successive interference cancellation. Furthermore, to set a benchmark, accurate analytical expressions and numerical results are provided to demonstrate the effectiveness of the NOMA-assisted MEC system over the orthogonal multiple access-based scheme. At the end, we provide the basic guidelines for choosing transceiver hardware that will meet the practical requirements of a CDRT-based uplink-NOMA transmission system for efficient offloading, where the performance of the MEC server is evaluated in terms of latency and energy consumption. The Monte Carlo simulations validate the accuracy of the derived analytical expressions.

INDEX TERMS Mobile edge computing, offloading delay, energy consumption, non-orthogonal multiple access, transceiver hardware impairments, ergodic sum capacity, outage probability.

I. INTRODUCTION

The rapid growth of resource-intensive mobile applications, such as smart health monitoring, automatic driving, augmented reality, virtual reality, and vehicular crowd sensing, is increasing in future-generation wireless systems [1], [2]. Usually, such applications are latency-sensitive and

computationally intensive, which results in a heavy computing load on mobile devices [2]. Since most mobile devices are small in size, it can be difficult to afford sophisticated smart applications locally, with reduced latency and less energy consumption. In recent times, mobile edge computing (MEC) has become one of the most promising solutions to meet the escalating demand for efficient computational services. Through the offloading of these computationally intensive tasks onto the MEC server via a base station (BS),

The associate editor coordinating the review of this manuscript and approving it for publication was Tao Zhou.

the gap between the limited functionality of mobile devices and the increasing demand for advanced functionality can be bridged [3], [4]. Specifically, MEC prolongs the battery life of mobile devices and enables devices to complete their tasks before the deadlines by preventing the devices from spending energy on local computing [3], [5], [6]. The MEC paradigm, while allowing efficient computational services, can potentially place the bottleneck in communication rather than computation. As a result, it becomes increasingly pertinent to incorporate efficient communication techniques into MEC frameworks in order to improve capacity and connectivity [7]. Additionally, the efficient use of data transmission networks can boost the performance of task offloading, which can reduce the operational costs for application vendors [8]. Meantime, with the requirement of high data rates and efficiency, multiple access techniques with a non-orthogonal approach, have been recognized as a promising solution for enhancing the spectral efficiency of mobile wireless networks [9]. In contrast to conventional orthogonal multiple access (OMA) schemes, non-orthogonal multiple access (NOMA) allows simultaneous service to multiple user equipment in the same degrees of freedom by splitting them in the power domain [10], [11], [12]. Multi-user OMA access techniques divvy up the system resources based on time, frequency, or code, while Multi-access NOMA allows users to use resources simultaneously on the same frequency with different power levels or code allocations in an orthogonal manner [10], [13]. It has been widely shown in the literature, that NOMA inspired MEC offloading can reduce the system latency and energy consumption, allowing it to be valuable and efficient in uplink transmission systems [3], [14].

In [5], using NOMA in the MEC system produced a significant reduction in energy consumption by optimizing transmit power control, transmission time allocations, and task offloading partitions. Moreover, [15] proposed a NOMA-MEC scheme with an assistant to minimize energy consumption and maximize data offloading by jointly optimizing communication and computing resources between users and assistants. Based on the results of [16], the study optimized both user offloading workload and transmission time in order to minimize the overall delay of the users. Furthermore, Sheng et al. examined how co-channel interference interacts with differential upload delay of NOMA users [17]. It has been studied somehow to minimize the weighted sum of time and energy consumption in a system, which is known as the system cost. According to Yang et al. [18], when upload data rate and edge computing capabilities are limited, the completion time of all tasks and the total energy consumption are minimized. Authors in [19] minimized the weighted value of time and energy consumption through joint optimization of the power and time allocation of each group. By optimizing offloading decisions, wireless power transfer durations, and transmission durations of offloading wireless devices, the authors in [20] well investigate the

energy-limited and computational capacity-limited problems of wireless devices. Meantime, the authors in [21] discussed a mobile wireless-powered communication network under an energy causality constraint that can maximize throughput if the energy consumption of one transmission is coupled with the probability of energy harvesting. The application of NOMA in wireless networks, makes the networks much more efficient at using spectrum, thanks to advanced transceiver designs like superposition coding and successive interference cancellation (SIC) [22], [23], [24]. Furthermore, the authors in [25] demonstrate that NOMA using coordinated direct and relay transmission (CDRT) produces significant performance gains when compared to NOMA in a non-CDRT cooperative framework, especially when the far user channel is in a heavily shadowed stage. In this context, an uplink and downlink cooperative NOMA (C-NOMA) with both direct and relayed links were proposed in order to further increase the efficiency of the earlier discussed systems [26], [27]. The authors of [27] and [28], estimated the ergodic sum capacity (ESC) of an uplink cooperative system using CDRT for both perfect and imperfect SIC. This paper provides an analysis of a NOMA-based MEC transmission system with the required coordinating support of a relay node to maintain the performance of a non-CDRT-based NOMA system when the maximum expected performance is insufficient to offer a good amount of system performance without considering CDRT. Coordinating directly with relaying can enhance signal-to-noise ratios (SNRs) in areas where transmission connectivity is limited, thereby enabling better sum capacity and less energy consumption with low latency in a NOMA-MEC framework.

In common with the aforementioned works, the perfect radio frequency (RF) components are assumed at the transceivers, which is an impractical approach for realistic systems. Practically, the hardware of all RF components may suffer from several types of impairments [29]. As a result, the transmitted signal has a mismatch with the intended signal, and the signal received is distorted as well. The presence of RF impairment may in turn, impair the quality of the modulated radio frequency (RF) signal due to non-linearities in high power amplifiers (HPA), in-phase/quadrature-phase imbalance (IQI) in modulators, resolution of analog-to-digital converter and phase noise (PN) of the oscillator [29], [30]. Even though some algorithms have been developed to mitigate such impairments, residual issues still persist. This limitation can lead to slower computation and execution of tasks, resulting in increased latency and reduced overall performance. Hardware impairments, such as limited network bandwidth or unreliable wireless connections, can cause delays and packet loss, leading to increased latency and reduced throughput [29], [31], [32]. In this respect, the performance of a C-NOMA under residual hardware impairment (RHIs), imperfect channel state information and imperfect SIC was evaluated in [33]. The works reported in [34], concern uplink NOMA-based

short packet communication in the presence of RHIs. While, the authors of [35] studied the effects of RHIs on an uplink NOMA-based MEC system with an imperfect SIC. Yet, there is still a lack of theoretical performance analysis, which will fill the research gap related to CDRT scheme for uplink NOMA-based MEC systems in the presence of RHIs.

Motivated by the aforementioned discussion, the purpose of this paper is to investigate the effects of RHIs and imperfect SICs on cooperative uplink CDRT-NOMA for task offloading on MEC networks, where the combined allocation of communication and computing resources results in improved end-user experience. The main contributions of this paper are summarized as follows:

- 1) An uplink CDRT-NOMA-based MEC system is presented and investigated, where a near or strong user (U1) directly communicates with a MEC server connected to a BS for computational-intensive task offloading, whereas, a far or weak user (U2) needs to communicate with the MEC server via decode and forward (DF) relay R in half-duplex mode.
- 2) For assessing the impact of transceiver RHIs, a closed-form solution of the ESC and outage probability (OP) of uplink-NOMA and the task offloading latency of users is derived under imperfect SIC. Energy consumption is evaluated based on the number of users and tasks assigned to the users for offloading in MEC assisted uplink-NOMA systems.
- 3) Through analytical analysis and numerical results, we demonstrate the superiority of uplink NOMA-based MEC systems over conventional multiple access schemes such as OMA.

The remainder of this paper is organized as follows. The system and channel model is illustrated in Section II. In Section III, closed-form expressions for the exact ESC and OP of the CDRT in uplink NOMA based MEC system suffering from imperfect SIC with RHI are derived. Numerical and simulation results are provided in Section IV. Finally, Section V concludes the paper.

II. SYSTEM AND CHANNEL MODEL

As illustrated in Fig. 1, we consider an uplink-NOMA aided communication system, which consists of a BS equipped with a single MEC server (i.e. gateway or base state) for user task offloading computation. In the task offloading duration, the MEC server selects two users, denoted by U1 and U2, one from the near group and the other from the far group, to perform uplink NOMA. The reason for making two groups (near and far group) is edge computing users accessing the same channel via uplink NOMA cause severe co-channel interference and increase the system complexity. Initially, we analyse a two-user scenario for the task offloading and later, numerous user pairs are taken into account for energy usage and latency. The paired user (user U1 and user U2), where the near user U1 directly communicates with the BS, and the far user U2 needs to communicate with the

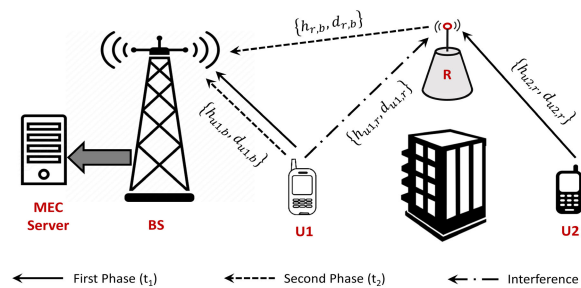


FIGURE 1. Proposed system model consisting of a BS, a DF relay (R), a cell-center user (U1), a cell-edge user (U2) and a MEC server.

BS via DF relay R. Further, owing to heavy shadowing problems or physical obstacles, we have assumed that the communication between U2 and BS is only through the relay node. At the BS and relay, SIC is used to separate the signals. Additionally, we assume that the channel for all the links is quasi-static, reciprocal, and subject to independent and identically distributed (i.i.d.) Rayleigh flat-fading with $E\{|h_{i,j}|^2\} = 1$, where $E\{\cdot\}$ denotes an expectation operator and $i, j \in \{U1, U2, R, BS\}$ with $i \neq j$. Therefore, the link gain $|h_{i,j}|^2$ is a random variable and exponentially distributed. Assume that, the complex fading channel coefficient $h_{i,j} \sim \mathcal{CN}(0, \lambda_{i,j} = d_{i,j}^{-\chi})$ is having zero mean and variance $\lambda_{i,j}$ between any two nodes i and j , where χ is the path loss exponent. In the following, subscripts $b, r, u1$, and $u2$ denote BS, relay, near user U1, and far user U2, respectively. Without loss of generality, the ordered user channel gains can be assumed as $\lambda_{u1,b} > \lambda_{r,b} > \lambda_{u2,b}$ i.e. U1 is assumed to have a better link quality compared with relay and U2 either in the first phase or second phase. Therefore, it is expected that $|h_{u1,b}|^2 > |h_{r,b}|^2 > |h_{u2,b}|^2$.

A. TASK OFFLOADING

In this paper, in two phases, both users offload their tasks to the MEC server with CDRT scheme. The following assumptions are considered: i) The computationally intensive latency-critical tasks of each user must be offloaded to the MEC server, due to the limited computational capabilities of users. The local computation can consume a considerable amount of time and energy, and also in many cases, users unable to complete their tasks by the deadlines, which is why MEC is used. ii) The computation time at the MEC server and the time for downloading the outcomes back to users are omitted due to the fact that MEC servers usually have a strong computing capability, and BS servers usually have high transmitting power [36]. iii) All the nodes have only one antenna and the transmission is half-duplex, with no node can transmit and receive simultaneously. Further assuming each user has L number of tasks, where each task is inseparable and the task τ belonging to user i contains $N_{i,\tau}$ bits. Performance of the considered system can be measured from a latency perspective as well as from an energy perspective with MEC is as follows:

i) *Latency of MEC*: Denote the data rate for user i to offload task τ by $R_{i,\tau}$ which is a function of the transmit power. In particular, denote the transmit power used by user i to offload task τ by $P_{i,\tau}$. The time required for offloading task τ of user i is given by [3]

$$T_{i,\tau} = \frac{N_{i,\tau}}{R_{i,\tau}} = \frac{N_{i,\tau}}{\sum_{\tau=1}^L B \log(1 + \gamma_{i,\tau})}, \quad (1)$$

where B is the bandwidth, $R_{i,\tau}$ is the task offloading rate and $\gamma_{i,\tau}$ is the corresponding signal interference plus distortion noise ratio (SIDNR) for $i \in \{u1, u2\}$ and defined under communication model.

Due to point of Assumption i), since all tasks are fully offloaded and hence local computing does not incur any delay cost.

ii) *Energy Consumption of MEC*: The total energy consumed by offloading all the L tasks of user i is given by [3]

$$E_i = \sum_{\tau=1}^L P_{i,\tau} T_{i,\tau} = \sum_{\tau=1}^L P_{i,\tau} \frac{N_{i,\tau}}{R_{i,\tau}} = \sum_{\tau=1}^L P_{i,\tau} \frac{N_{i,\tau}}{\sum_{\tau=1}^L B \log(1 + \gamma_{i,\tau})}. \quad (2)$$

Without loss of generality, assume that m users are offloading their tasks as follows: $|h_1|^2 \leq \dots \leq |h_m|^2$, where h_m is the channel gain between user m and MEC server. m is the number of users $m=2M$, where M is the number of user pair and $M > 0$. It may be possible to implement OMA-MEC and NOMA-MEC in the following ways if the users' tasks are delay-sensitive i.e. saving offloading time has higher priority than deducing energy consumption.

Each user is allocated a specific time slots for offloading its tasks to the MEC server in OMA-MEC i.e. for task offloading, each user needs the following time interval:

$$T_i = \frac{N}{\log(1 + \gamma_{i,OMA})} \quad (3)$$

assuming $N = N_{i,1}$ i.e same number of nats (size) for all users and single task for offloading ($L = 1$) to facilitate the performance.

In NOMA-MEC, both the users can offload their tasks simultaneously. The task offloading process does not require extra time for user U1, hence offloading latency is reduced

$$T_i = \frac{N}{\log(1 + \gamma_{i,NOMA})}. \quad (4)$$

B. COMMUNICATION MODEL

1) FIRST PHASE (T_1)

We depict in Fig. 1, a paired user (U1 and U2) of M number of pairs communicates in two phases with the BS using CDRT. According to the principle of uplink-NOMA [11], [37], user U1 and U2 transmit symbols x_1 and y_1 simultaneously with powers a_1P and a_2P respectively, where P indicates the

total transmit power and a_1 and a_2 are the power allocation coefficients. In this paper, U1 and U2 transmit their signals non-orthogonally with constrained of total transmitted power [37] and hence $a_1 + a_2 = 1$. The received signal at the BS in the presence of RHI can be expressed as [38], [39], and [40]

$$y_b(t_1) = \sqrt{a_1 P} h_{u1,b} x_1(t_1) + \eta_b(t_1) + n_b(t_1), \quad (5)$$

where $n_b(t_1)$ denotes the additive white Gaussian noise (AWGN) with zero-mean and variance N_0 , i.e. $n_b(t_1) \sim \mathcal{CN}(0, N_0)$. $\eta_b(t_1) \sim \mathcal{CN}(0, k_a^2 a_1 P |h_{u1,b}|^2)$, is the aggregated distortion noises from impairments in the transmitter and receiver [39], [40]. Theoretical investigations and measurements (e.g., [39], [40]) have shown that

$$\eta_{tx} \sim \mathcal{CN}(0, k_{tx}^2 P) \text{ \& } \eta_{rx} \sim \mathcal{CN}(0, k_{rx}^2 P |h|^2). \quad (6)$$

η_{tx}, η_{rx} are distortion noises from impairments in the transmitter and receiver. The design parameters $k_{tx}, k_{rx} \geq 0$ characterize the level of impairments in the transmitter and receiver hardware, respectively.

Remark 1: The distortions from transceiver impairments act as an additional noise source of variance $(k_{tx}^2 + k_{rx}^2)P|h|^2$. Thus, it is sufficient to determine the aggregate level of impairments $k_a = \sqrt{(k_{tx}^2 + k_{rx}^2)}$. We consider the aggregated hardware impairments at all the receivers' end. The analysis can be readily generalized by k_a -parameters in our setup as the aggregate parameters for each link.

Now using (5), the effective signal to distortion and noise ratio at BS for detection of the symbol x_1 is given by

$$\gamma_{b,x_1}^{t_1} = \frac{a_1 \rho |h_{u1,b}|^2}{a_1 \rho k_a^2 |h_{u1,b}|^2 + 1}, \quad (7)$$

where $\rho = \frac{P}{N_0}$ is the transmit signal-to-noise ratio (SNR).

The ergodic rate of U1 is therefore given as

$$R_{x_1}^{t_1} = \frac{1}{2} \log_2 \left(1 + \frac{a_1 \rho |h_{u1,b}|^2}{a_1 \rho k_a^2 |h_{u1,b}|^2 + 1} \right), \quad (8)$$

by assuming the time synchronization between user 1 and 2. The signal received at the relay node R is given by

$$y_r(t_1) = \sqrt{a_1 P} h_{u1,r} x_1(t_1) + \sqrt{a_2 P} h_{u2,r} y_1(t_1) + \eta_r(t_1) + n_r(t_1), \quad (9)$$

where $n_r(t_1) \sim \mathcal{CN}(0, N_0)$ denotes the AWGN and $\eta_r(t_1) \sim \mathcal{CN}(0, k_a^2 (a_1 P |h_{u1,r}|^2 + a_2 P |h_{u2,r}|^2))$ is the aggregated distortion noises from impairments.

According to the principle of uplink-NOMA, R can decode the symbol x_1 of U1 and y_1 of U2 by using SIC and also taking following two cases into consideration.

i) Case-1: $\lambda_{u1,r} > \lambda_{u2,r}$

In light of the principle of uplink-NOMA, R first decodes the symbol x_1 subject to the better link quality by treating the symbol y_1 subject to the inferior link quality as noise.

Note: In uplink-NOMA, decoding order always begins with the users with better channels and ending with the users

with worse channels. Using (9), the received SIDNRs for R to detect x_1 and y_1 are respectively expressed as

$$\gamma_{r,x_1,1}^{t_1} = \frac{a_1 \rho |h_{u1,r}|^2}{a_2 \rho (1 + k_a^2) |h_{u2,r}|^2 + a_1 \rho k_a^2 |h_{u1,r}|^2 + 1} \quad (10)$$

and

$$\gamma_{r,y_1,1}^{t_1} = \frac{a_2 \rho |h_{u2,r}|^2}{a_1 \rho |\tilde{g}_{u1,r}|^2 + a_1 \rho k_a^2 |h_{u1,r}|^2 + a_2 \rho k_a^2 |h_{u2,r}|^2 + 1} \\ = \frac{a_2 \rho |h_{u2,r}|^2}{a_1 \rho (k_1 + k_a^2) |h_{u1,r}|^2 + a_2 \rho k_a^2 |h_{u2,r}|^2 + 1}, \quad (11)$$

where $\tilde{g}_{u1,r} \sim \mathcal{CN}(0, k_1 \lambda_{u1,r})$ and the parameter $k_1 (0 \leq k_1 \leq 1)$ indicate the level of residual interference due to imperfect SIC at R. A special case, $k_1 = 0$ denotes perfect SIC, whereas $k_1 = 1$ indicates that no SIC is performed at relay node. Similarly, the parameter $k_a (0 \leq k_a \leq 1)$ indicates the level of residual interference due to hardware impairments at R and for $k_a = 0$, denotes no RHI, whereas $k_a = 1$, denotes the presence of RHI at Relay node. The ergodic rate of U2 is given as

$$R_{y_1,1}^{t_1} = \frac{1}{2} \log_2(1 + \gamma_{r,y_1,1}^{t_1}). \quad (12)$$

ii) Case-2: $\lambda_{u1,r} < \lambda_{u2,r}$

Relay node first decodes the symbol y_1 subject to the better link quality by treating the symbol x_1 subject to the inferior link quality as noise. Using (9), the received SIDNRs for R to detect y_1 is given as

$$\gamma_{r,y_1,2}^{t_1} = \frac{a_2 \rho |h_{u2,r}|^2}{a_1 \rho (1 + k_a^2) |h_{u1,r}|^2 + a_2 \rho k_a^2 |h_{u2,r}|^2 + 1}. \quad (13)$$

The ergodic rate of U2 is given by

$$R_{y_1,2}^{t_1} = \frac{1}{2} \log_2(1 + \gamma_{r,y_1,2}^{t_1}). \quad (14)$$

2) SECOND PHASE (T_2)

U1 and R re-transmits the new data symbol x_2 and decoded symbol y_1 with power a_3P and a_4P respectively, where a_3 and a_4 are the new power allocation factor with $a_3 + a_4 = 1$. The received signal at the BS in the presence of RHI can be expressed as

$$y_b(t_2) = \sqrt{a_3 P} h_{u1,b} x_2(t_2) + \sqrt{a_4 P} h_{r,b} y_1(t_2) \\ + \eta_b(t_2) + n_b(t_2), \quad (15)$$

where $n_b(t_2) \sim \mathcal{CN}(0, N_0)$ denotes the AWGN and $\eta_b(t_2) \sim \mathcal{CN}(0, k_a^2(a_3P|h_{u1,b}|^2 + a_4P|h_{r,b}|^2))$ is the aggregated distortion noise from impairments. Using the concept of uplink-NOMA, the symbol x_2 is decoded first by treating y_1 as noise. Then, BS performs SIC to decode y_1 . The received SIDNRs for BS to detect x_2 and y_1 are respectively given by

$$\gamma_{b,x_2}^{t_2} = \frac{a_3 \rho |h_{u1,b}|^2}{a_4 \rho (1 + k_a^2) |h_{r,b}|^2 + a_3 \rho k_a^2 |h_{u1,b}|^2 + 1} \quad (16)$$

and

$$\gamma_{b,y_1}^{t_2} = \frac{a_4 \rho |h_{r,b}|^2}{a_3 \rho |\tilde{g}_{u1,b}|^2 + a_3 \rho k_a^2 |h_{u1,b}|^2 + a_4 \rho k_a^2 |h_{r,b}|^2 + 1} \\ = \frac{a_4 \rho |h_{r,b}|^2}{a_3 \rho (k_2 + k_a^2) |h_{u1,b}|^2 + a_4 \rho k_a^2 |h_{r,b}|^2 + 1}, \quad (17)$$

where $\tilde{g}_{u1,b} \sim \mathcal{CN}(0, k_2 \lambda_{u1,b})$ and the parameter $k_2 (0 \leq k_2 \leq 1)$ indicates the level of residual interference due to imperfect SIC at BS. A special case, $k_2 = 0$ denotes perfect SIC, whereas $k_2 = 1$ indicates that no SIC is performed at BS. Similarly the parameter $k_a (0 \leq k_a \leq 1)$ indicates the level of residual interference due to hardware impairments at BS and for $k_a = 0$ denotes no RHI, whereas $k_a = 1$ denotes the presence of RHI at BS.

Hence, the achievable ergodic rates of U1 and U2 are respectively given by

$$R_{x_2}^{t_2} = \frac{1}{2} \log_2(1 + \gamma_{b,x_2}^{t_2}) \quad (18)$$

and

$$R_{y_1}^{t_2} = \frac{1}{2} \log_2(1 + \gamma_{b,y_1}^{t_2}). \quad (19)$$

III. PERFORMANCE ANALYSIS

The closed-form solution of the ESC and OP of uplink-NOMA-MEC over Rayleigh fading channels is given in this section.

A. SUM CAPACITY

The sum capacity of U1 by using (8) and (18) is given as

$$R_c^{u1} = R_{x_1}^{t_1} + R_{x_2}^{t_2} \quad (20)$$

The minimum one of the two hops of a dual-hop cooperative links is the end-to-end capacity and using (12), (14) and (19) the capacity of U2 is obtained as

$$R_c^{u2} = \begin{cases} \min(R_{y_1,1}^{t_1}, R_{y_1}^{t_2}) = \frac{1}{2} \log_2(1 + \min(\gamma_{r,y_1,1}^{t_1}, \gamma_{b,y_1}^{t_2})), & \text{Case-1} \\ \min(R_{y_1,2}^{t_1}, R_{y_1}^{t_2}) = \frac{1}{2} \log_2(1 + \min(\gamma_{r,y_1,2}^{t_1}, \gamma_{b,y_1}^{t_2})), & \text{Case-2} \end{cases} \quad (21)$$

Now using (20) and (21), the sum capacity of uplink-NOMA-MEC with RHI is expressed as

$$R_c^{sum} = R_c^{u1} + R_c^{u2}. \quad (22)$$

i) Ergodic Capacity (EC) of U1

Let $Z_1 = \gamma_{b,x_1}^{t_1}$ and $Z_2 = \gamma_{b,x_2}^{t_2}$. The cumulative distribution function (CDF) of Z_1 can be expressed as in [41, Eq. (22)]

$$F_{Z_1}(z_1) = 1 - \frac{A}{A + B z_1} e^{-\frac{z_1}{A}} \\ = 1 - \frac{a_1 \rho \lambda_{u1,b}}{a_1 \rho \lambda_{u1,b} + a_1 \rho k_a^2 \lambda_{u1,b} z_1} e^{-\frac{z_1}{a_1 \rho \lambda_{u1,b}}} \\ = 1 - \frac{1}{1 + k_a^2 z_1} e^{-\frac{z_1}{a_1 \rho \lambda_{u1,b}}}. \quad (23)$$

Further, the CDF of Z_2 can be expressed as in [41, Eq.(22)]

$$F_{Z_2}(z_2) = 1 - \frac{a_3 \rho \lambda_{u1,b}}{a_3 \rho \lambda_{u1,b} + a_4 \rho (1 + k_a^2) \lambda_{r,b} z_2} \times \frac{a_3 \rho \lambda_{u1,b}}{a_3 \rho \lambda_{u1,b} + a_3 \rho k_a^2 \lambda_{u1,b} z_2} e^{-\frac{z_2}{a_3 \rho \lambda_{u1,b}}} = 1 - \frac{k}{k + z_2} \times \frac{l}{l + z_2} e^{-\frac{z_2}{a_3 \rho \lambda_{u1,b}}}, \quad (24)$$

where $k = a_3 \lambda_{u1,b} / a_4 (1 + k_a^2) \lambda_{r,b}$ and $l = a_3 \lambda_{u1,b} / a_3 k_a^2 \lambda_{u1,b} = 1 / k_a^2$. By using (20), the EC of U1 is expressed as

$$\begin{aligned} \tilde{R}_c^{u1} &= E \{R_{x_1}^{t_1}\} + E \{R_{x_2}^{t_2}\} \\ &= \underbrace{\frac{1}{2} \int_0^\infty \log_2(1 + z_1) f_{Z_1}(z_1) dz_1}_{I_1} \\ &\quad + \underbrace{\frac{1}{2} \int_0^\infty \log_2(1 + z_2) f_{Z_2}(z_2) dz_2}_{I_2}. \end{aligned} \quad (25)$$

Using $\int_0^\infty \log_2(1 + z) f_Z(z) dz = \frac{1}{\ln 2} \int_0^\infty \frac{1 - F_Z(z)}{1 + z} dz$, (26) is obtained as

$$\begin{aligned} \tilde{R}_c^{u1} &= \frac{\log_2 e}{2} \frac{1}{(1 - k_a^2)} \left[\left\{ -e^{-\left(\frac{1}{a_1 \rho \lambda_{u1,b}}\right)} Ei\left(-\frac{1}{a_1 \rho \lambda_{u1,b}}\right) \right\} \right. \\ &\quad \left. + \left\{ e^{\left(\frac{1}{a_1 \rho k_a^2 \lambda_{u1,b}}\right)} Ei\left(-\frac{1}{a_1 \rho k_a^2 \lambda_{u1,b}}\right) \right\} \right] \\ &\quad + \frac{\log_2 e}{2} \frac{k}{(k - 1)} \left[\frac{1}{l - 1} \left\{ -e^{m_1} Ei(-m_1) \right\} \right. \\ &\quad \left. + \frac{1}{l - k} \left\{ -e^{km_1} Ei(-km_1) \right\} \right], \end{aligned} \quad (27)$$

where $m_1 = \frac{1}{a_3 \rho \lambda_{u1,b}}$ and $Ei(\cdot)$ indicates the exponential integral function [42], [43] and is expressed by

$$Ei(\beta) = \frac{(-\beta)^{\delta-1}}{(\delta - 1)!} [-\ln \beta + \psi(\delta)] - \sum_{\tau=0}^{\infty} \frac{(-\beta)^\tau}{(\tau - \delta + 1)\tau!},$$

with $\begin{cases} \psi(1) = -\varepsilon \\ \psi(\delta) = -\varepsilon + \sum_{\tau=1}^{\delta-1} \frac{1}{\tau} \end{cases} \quad \delta > 1,$

where $\varepsilon \approx 0.577$ is the Euler constant and $(\delta \in \{N, F, b\})$. From (27), we observed that \tilde{R}_c^{u1} linearly increases with the increasing of transmit SNR (ρ).

Proof: See Appendix A.

Proposition 1: With ideal hardware (*i.e.* $k_a = 0$), the exact EC of U1 is given as

$$\tilde{R}_{c,ideal}^{u1} = \frac{\log_2 e}{2} \left[-e^{\frac{1}{a_1 \rho \lambda_{u1,b}}} Ei\left(-\frac{1}{a_1 \rho \lambda_{u1,b}}\right) + \frac{a_3 \lambda_{u1,b}}{a_3 \lambda_{u1,b} - a_4 \lambda_{r,b}} \times \left\{ -e^{\frac{1}{a_3 \rho \lambda_{u1,b}}} Ei\left(-\frac{1}{a_3 \rho \lambda_{u1,b}}\right) \right\} + e^{\frac{1}{a_4 \rho \lambda_{r,b}}} Ei\left(-\frac{1}{a_4 \rho \lambda_{r,b}}\right) \right]. \quad (28)$$

Proof: With ideal hardware, Z_1 and Z_2 can be re-written as $Z_1 = \gamma_{x_1}^{t_1} = a_1 \rho |h_{u1,b}|^2$ and $Z_2 = \gamma_{b,x_2}^{t_2} = \frac{a_3 \rho |h_{u1,b}|^2}{a_4 \rho |h_{r,b}|^2 + 1}$. The CDF of Z_1 and Z_2 are respectively given as

$$F_{Z_1}(z_1) = 1 - e^{-\frac{z_1}{a_1 \rho \lambda_{u1,b}}} \quad (29)$$

and

$$F_{Z_2}(z_2) = 1 - \frac{a_3 \rho \lambda_{u1,b}}{a_3 \rho \lambda_{u1,b} + a_4 \rho \lambda_{r,b} z_2} e^{-\frac{z_2}{a_3 \rho \lambda_{u1,b}}}. \quad (30)$$

Using (29), (30) and $\int_0^\infty \log_2(1+z) f_Z(z) dz = \frac{1}{\ln 2} \int_0^\infty \frac{1 - F_Z(z)}{1+z} dz$, the exact EC of U1 is obtained as (28).

ii) *EC of U2*

Considering Case-1 and Case-2, the closed-form solution of the EC for U2 is obtained as follows

1) Case-1: Let $Z_3 = \gamma_{r,y_1}^{t_1}$, $Z_4 = \gamma_{b,y_1}^{t_2}$, and $V = \min(Z_3, Z_4)$. The CDF of Z_3 and Z_4 can be respectively expressed as

$$F_{Z_3}(z_3) = 1 - \frac{a_2 \rho \lambda_{u2,r}}{a_2 \rho \lambda_{u2,r} + a_1 \rho (k_1 + k_a^2) \lambda_{u1,r} z_3} \times \frac{a_2 \rho \lambda_{u2,r}}{a_2 \rho \lambda_{u2,r} + a_2 \rho k_a^2 \lambda_{u2,r} z_3} e^{-\frac{z_3}{a_2 \rho \lambda_{u2,r}}} = 1 - \frac{p}{p + z_3} \times \frac{q}{q + z_3} e^{-\frac{z_3}{a_2 \rho \lambda_{u2,r}}}, \quad (31)$$

where $p = \frac{a_2 \lambda_{u2,r}}{a_1 (k_1 + k_a^2) \lambda_{u1,r}}$, $q = \frac{1}{k_a^2}$ and

$$F_{Z_4}(z_4) = 1 - \frac{a_4 \rho \lambda_{r,b}}{a_3 \rho \lambda_{r,b} + a_3 \rho (k_2 + k_a^2) \lambda_{u1,b} z_4} \times \frac{a_4 \rho \lambda_{r,b}}{a_4 \rho \lambda_{r,b} + a_4 \rho k_a^2 \lambda_{r,b} z_4} e^{-\frac{z_4}{a_4 \rho \lambda_{r,b}}} = 1 - \frac{s}{s + z_4} \times \frac{t}{t + z_4} e^{-\frac{z_4}{a_4 \rho \lambda_{r,b}}}, \quad (32)$$

where $s = \frac{a_4 \lambda_{r,b}}{a_3 (k_2 + k_a^2) \lambda_{u1,b}}$ and $t = \frac{1}{k_a^2}$. Using (31) and (32) the CDF of V can be written by

$$F_V(v) = 1 - \frac{p}{p + v} \times \frac{q}{q + v} \times \frac{s}{s + v} \times \frac{t}{t + v} e^{-m_2 v}, \quad (33)$$

where $m_2 = \frac{1}{a_2 \rho \lambda_{u2,r}} + \frac{1}{a_4 \rho \lambda_{r,b}}$. Hence the EC of U2 is expressed as

$$\begin{aligned} \tilde{R}_{c,1}^{u2} &= E \{R_{c,1}^{u2}\} \\ &= \frac{1}{2} \int_0^\infty \log_2(1 + v) f_V(v) dv \\ &= \frac{\log_2 e}{2} \int_0^\infty (1 + v)^{-1} \frac{p}{p + v} \times \frac{q}{q + v} \times \frac{s}{s + v} \times \frac{t}{t + v} e^{-m_2 v} dv \\ &= g_1 \frac{t}{t - 1} \{ -e^{m_2} Ei(-m_2) + e^{tm_2} Ei(-tm_2) \} \\ &\quad - g_1 \frac{t}{t - s} \{ -e^{sm_2} Ei(-sm_2) + e^{tm_2} Ei(-tm_2) \} \\ &\quad - g_2 \frac{t}{t - q} \{ -e^{qm_2} Ei(-qm_2) + e^{tm_2} Ei(-tm_2) \} \\ &\quad + g_2 \frac{t}{t - s} \{ -e^{sm_2} Ei(-sm_2) + e^{tm_2} Ei(-tm_2) \} \end{aligned}$$

$$\begin{aligned}
& -g_3 \frac{t}{t-p} \left\{ -e^{pm_2} Ei(-pm_2) + e^{tm_2} Ei(-tm_2) \right\} \\
& -g_3 \frac{t}{t-s} \left\{ -e^{sm_2} Ei(-sm_2) + e^{tm_2} Ei(-tm_2) \right\} \\
& -g_4 \frac{t}{t-q} \left\{ -e^{qm_2} Ei(-qm_2) + e^{tm_2} Ei(-tm_2) \right\} \\
& +g_4 \frac{t}{t-s} \left\{ -e^{sm_2} Ei(-sm_2) + e^{tm_2} Ei(-tm_2) \right\},
\end{aligned} \tag{34}$$

where $g = \frac{p}{p-1} \frac{\log_2 e}{2}$, $g_1 = g \frac{q}{q-1} \frac{s}{s-1}$, $g_2 = g \frac{q}{q-1} \frac{s}{s-q}$, $g_3 = g \frac{q}{q-p} \frac{s}{s-p}$ and $g_4 = g \frac{q}{q-p} \frac{s}{s-q}$.

Proof: See Appendix B

Looking to (34), we observe that under non-ideal hardware and imperfect SIC, k_a , k_1 and k_2 have significant impact on the EC of U2. The EC of U2 decreases with increasing k_a , k_1 and/or k_2 , and vice versa. The exact EC of U2 under ideal hardware and perfect SIC is given in the below proposition.

Proposition 2: With ideal hardware (i.e. $k_a = 0$) and with perfect SIC (i.e. $k_1 = k_2 = 0$), the exact EC of U2 is given by

$$\tilde{R}_{c,1,ideal}^{p,u2} = -\frac{\log_2 e}{2} e^{m_2} Ei(-m_2). \tag{35}$$

Proof: With ideal hardware and with perfect SIC, $V = \min(\gamma_{r,y_1}^{t_1}, \gamma_{b,y_1}^{t_2})$ can be written as $V = \min(a_2 \rho |h_{u2,r}|^2, a_4 \rho |h_{r,b}|^2)$. So the CDF of V can be given as

$$F_V(v) = 1 - e^{-\frac{1}{a_2 \rho |h_{u2,r}|^2} v - \frac{1}{a_4 \rho |h_{r,b}|^2} v}. \tag{36}$$

Using $\int_0^\infty \log_2(1+z) f_Z(z) dz = \frac{1}{\ln 2} \int_0^\infty \frac{1-F_Z(z)}{1+z} dz$, the exact EC of U2 is acquired as (35).

2) Case-2: Let $W = \min(\gamma_{r,y_1,2}^{t_1}, \gamma_{b,y_1}^{t_2})$ and following the similar steps to evaluate (34), the exact EC of U2 under imperfect SIC and non-ideal hardware can be given as

$$\begin{aligned}
\tilde{R}_{c,2}^{u2} &= E \left\{ R_{c,2}^{u2} \right\} \\
&= h_1 \frac{t}{t-1} \left\{ -e^{m_2} Ei(-m_2) + e^{tm_2} Ei(-tm_2) \right\} \\
&\quad - h_1 \frac{t}{t-s} \left\{ -e^{sm_2} Ei(-sm_2) + e^{tm_2} Ei(-tm_2) \right\} \\
&\quad - h_2 \frac{t}{t-q} \left\{ -e^{qm_2} Ei(-qm_2) + e^{tm_2} Ei(-tm_2) \right\} \\
&\quad + h_2 \frac{t}{t-s} \left\{ -e^{sm_2} Ei(-sm_2) + e^{tm_2} Ei(-tm_2) \right\} \\
&\quad - h_3 \frac{t}{t-n} \left\{ -e^{nm_2} Ei(-nm_2) + e^{tm_2} Ei(-tm_2) \right\} \\
&\quad - h_3 \frac{t}{t-s} \left\{ -e^{sm_2} Ei(-sm_2) + e^{tm_2} Ei(-tm_2) \right\} \\
&\quad - h_4 \frac{t}{t-q} \left\{ -e^{qm_2} Ei(-qm_2) + e^{tm_2} Ei(-tm_2) \right\} \\
&\quad + h_4 \frac{t}{t-s} \left\{ -e^{sm_2} Ei(-sm_2) + e^{tm_2} Ei(-tm_2) \right\},
\end{aligned} \tag{37}$$

where $n = \frac{a_2 \lambda_{u2,r}}{a_1(1+k_a^2) \lambda_{u1,r}}$, $h = \frac{n}{n-1} \frac{\log_2 e}{2}$, $h_1 = h \frac{q}{q-1} \frac{s}{s-1}$, $h_2 = h \frac{q}{q-1} \frac{s}{s-q}$, $h_3 = h \frac{q}{q-n} \frac{s}{s-n}$ and $h_4 = h \frac{q}{q-n} \frac{s}{s-q}$.

Looking to (37), we notice that under non-ideal hardware and imperfect SIC, k_a and k_2 have a significant impact on the EC of U2. With increasing k_a and k_2 , EC of U2 may decrease and vice versa. The exact EC of U2 with ideal hardware and perfect SIC is given in the below proposition.

Proposition 3: With ideal hardware (i.e. $k_a = 0$) and with perfect SIC (i.e. $k_2 = 0$) the exact EC of U2 is given as

$$\tilde{R}_{c,2,ideal}^{p,u2} = \frac{n \log_2 e}{2(n-1)} \left\{ -e^{m_2} Ei(-m_2) + e^{nm_2} Ei(-nm_2) \right\}. \tag{38}$$

Proof: With ideal hardware and with perfect SIC, $W = \min(\gamma_{r,y_1,2}^{t_1}, \gamma_{b,y_1}^{t_2})$ can be written as $W = \min(\frac{a_2 \rho |h_{u2,r}|^2}{a_1 \rho |h_{u1,r}|^2 + 1}, a_4 \rho |h_{r,b}|^2)$. So the CDF of W can be given as

$$F_W(w) = 1 - \frac{a_2 \lambda_{u2,r}}{a_2 \lambda_{u2,r} + a_1 \lambda_{u1,r} w} e^{-\frac{1}{a_2 \rho |h_{u2,r}|^2} w - \frac{1}{a_4 \rho |h_{r,b}|^2} w}. \tag{39}$$

Using the same steps to derive (37), the exact EC of U2 in Case-2 with ideal hardware and perfect SIC is expressed as (38).

B. ESC OF UPLINK-NOMA-MEC

Using (27), (34) and (37), the ESC of uplink-NOMA CDRT based MEC with both RHI and imperfect SIC is expressed as

$$R_c^{sum} = \begin{cases} \tilde{R}_c^{u1} + \tilde{R}_{c,1}^{u2} & \text{Case - 1} \\ \tilde{R}_c^{u1} + \tilde{R}_{c,2}^{u2} & \text{Case - 2} \end{cases} \tag{40}$$

and using (28), (35) and (38), the ESC under both ideal hardware and perfect SIC is expressed as

$$R_c^{sum} = \begin{cases} \tilde{R}_{c,ideal}^{u1} + \tilde{R}_{c,1,ideal}^{p,u2} & \text{Case - 1} \\ \tilde{R}_{c,ideal}^{u1} + \tilde{R}_{c,2,ideal}^{p,u2} & \text{Case - 2.} \end{cases} \tag{41}$$

C. ESC OF UPLINK-OMA-MEC

To draw a fair comparison with uplink-NOMA, an uplink-OMA scheme with time-division multiple access is proposed. A mathematical expression for the ESC of OMA is given below.

$$\begin{aligned}
R_{OMA}^{sum} &= \frac{1}{4} \log_2(1 + \gamma_{b,x_1}^{t_1}) + \frac{1}{4} \log_2(1 + \gamma_{b,x_2}^{t_2}) \\
&\quad + \frac{1}{4} \log_2(1 + \min(\gamma_{r,y_1}^{t_1}, \gamma_{b,y_1}^{t_2})),
\end{aligned} \tag{42}$$

where $\gamma_{b,x_1}^{t_1} = \frac{\rho |h_{u1,b}|^2}{\rho k_a^2 |h_{u1,b}|^2 + 1}$, $\gamma_{b,x_2}^{t_2} = \frac{\rho |h_{u1,b}|^2}{\rho k_a^2 |h_{u1,b}|^2 + 1}$, $\gamma_{r,y_1}^{t_1} = \frac{\rho |h_{u2,r}|^2}{\rho k_a^2 |h_{u2,r}|^2 + 1}$ and $\gamma_{b,y_1}^{t_2} = \frac{\rho |h_{r,b}|^2}{\rho k_a^2 |h_{r,b}|^2 + 1}$.

D. OUTAGE PERFORMANCE ANALYSIS OF UPLINK-NOMA-MEC

The symbols x_1 and x_2 of U1 are transmitted at pre-defined objective rate R_1 in first and second phase, and the symbol y_1 of U2 is transmitted at pre-defined objective rate R_2 . The outage phenomenon occurred when the user instantaneous SIDNR falls below a pre-determined threshold. Under the presence of transceiver impairments and imperfect SIC, this

section derives new closed-form expressions for the precise OPs. The OP is denoted by $P_O(x)$ and it measures the probability that the end-to-end effective SIDNR falls below a certain threshold x , of acceptable communication quality.

At the BS, an outage occurs if the symbols x_1 and x_2 fail to be detected in first and second phases, respectively. Hence, the OPs using (7), (16) and [41, Eq.(22)] are respectively expressed as follows

$$\begin{aligned}
 P_O^{x_1}(x) &= P_r(\gamma_{b,x_1}^{t_1} \leq x) \\
 &= 1 - \frac{a_1 \rho \lambda_{u1,b}}{a_1 \rho \lambda_{u1,b} + a_1 \rho k_a^2 \lambda_{u1,b} x} e^{-\frac{x}{a_1 \rho \lambda_{u1,b}}} \\
 &= 1 - \frac{1}{1 + k_a^2 x} e^{-\frac{x}{a_1 \rho \lambda_{u1,b}}} \quad (43)
 \end{aligned}$$

and

$$\begin{aligned}
 P_O^{x_2}(x) &= P_r(\gamma_{b,x_2}^{t_2} \leq x) \\
 &= 1 - \frac{a_3 \rho \lambda_{u1,b}}{a_3 \rho \lambda_{u1,b} + a_3 \rho k_a^2 \lambda_{u1,b} x} \\
 &\quad \times \frac{a_3 \rho \lambda_{u1,b}}{a_3 \rho \lambda_{u1,b} + a_4 \rho (1 + k_a^2) \lambda_{r,b} x} e^{-\frac{x}{a_1 \rho \lambda_{u1,b}}} \\
 &= 1 - \frac{1}{1 + k_a^2 x} \frac{k}{k + x} e^{-\frac{x}{a_1 \rho \lambda_{u1,b}}}, \quad (44)
 \end{aligned}$$

where pre-fixed threshold rate for U1 $x = 2^{2R_1} - 1$.

Relay and BS failure occur when y_1 symbol is not detected during first and second phase, respectively under Case-1 and is given as

$$P_{O,y_1}^1(y) = P_r \left\{ \min(\gamma_{r,y_1,1}^{t_1}, \gamma_{b,y_1}^{t_2}) \leq y \right\}.$$

using (33),

$$P_{O,y_1}^1(y) = 1 - \frac{p}{p+y} \times \frac{q}{q+y} \times \frac{s}{s+y} \times \frac{t}{t+y} e^{-m_2 y}, \quad (45)$$

where pre-determined threshold rate for U2, $y = 2^{2R_2} - 1$.

Hence, OP of uplink-NOMA-MEC with RHI and imperfect SIC under Case-1 is given by

$$P_O^1 = P_O^{x_1} \times P_O^{x_2} \times P_{O,y_1}^1. \quad (46)$$

Following the similar steps to Case-1, under Case-2, outage occurs at Relay and BS when fails to detect the symbol y_1 in first and second phase, respectively, and is given as

$$\begin{aligned}
 P_{O,y_1}^2(y) &= P_r \left\{ \min(\gamma_{r,y_1,2}^{t_1}, \gamma_{b,y_1}^{t_2}) \leq y \right\} \\
 &= 1 - \frac{n}{n+y} \times \frac{q}{q+y} \times \frac{s}{s+y} \times \frac{t}{t+y} e^{-m_2 y} \quad (47)
 \end{aligned}$$

Similarly, OP of uplink-NOMA-MEC with RHI and imperfect SIC under Case-2 is given by

$$P_O^2 = P_O^{x_1} \times P_O^{x_2} \times P_{O,y_1}^2 \quad (48)$$

Proposition 4: With ideal hardware (i.e., $k_a = 0$) and with perfect SIC (i.e. $k_1 = k_2 = 0$), the exact OPs under Case-1 for the symbols x_1 , x_2 and y_1 are respectively given as

$$P_O^{p,x_1}(x) = P_r(\gamma_{b,x_1}^{t_1} \leq x) = 1 - e^{-\frac{x}{a_1 \rho \lambda_{u1,b}}} \quad (49)$$

$$\begin{aligned}
 P_O^{p,x_2}(x) &= P_r(\gamma_{b,x_2}^{t_2} \leq x) \\
 &= 1 - \frac{a_3 \rho \lambda_{u1,b}}{a_3 \rho \lambda_{u1,b} + a_4 \rho \lambda_{r,b} x} e^{-\frac{x}{a_1 \rho \lambda_{u1,b}}} \quad (50)
 \end{aligned}$$

and

$$P_{O,y_1}^{p,1}(y) = P_r \left\{ \min(\gamma_{r,y_1,1}^{t_1}, \gamma_{b,y_1}^{t_2}) \leq y \right\} = 1 - e^{-m_2 y} \quad (51)$$

where $\gamma_{b,x_1}^{t_1} = a_1 \rho \lambda_{u1,b}$, $\gamma_{b,x_2}^{t_2} = a_3 \rho \lambda_{u1,b} / a_4 \rho \lambda_{r,b} + 1$, $\gamma_{r,y_1,1}^{t_1} = a_2 \rho \lambda_{u2,r}$ and $\gamma_{b,y_1}^{t_2} = a_4 \rho \lambda_{r,b}$.

Hence, OP of uplink-NOMA-MEC with ideal hardware and perfect SIC under Case-1 is given as

$$P_O^{p,1} = P_O^{p,x_1} \times P_O^{p,x_2} \times P_{O,y_1}^{p,1}. \quad (52)$$

Similarly, the exact OPs under Case-2 for the symbols x_1 and x_2 are same as Case-1 and for the symbol y_1 is given as

$$\begin{aligned}
 P_{O,y_1}^{p,2}(y) &= P_r \left\{ \min(\gamma_{r,y_1,2}^{t_1}, \gamma_{b,y_1}^{t_2}) \leq y \right\} \\
 &= 1 - \frac{a_2 \rho \lambda_{u2,r}}{a_2 \rho \lambda_{u2,r} + a_1 \rho \lambda_{u1,r} y} e^{-m_2 y}, \quad (53)
 \end{aligned}$$

where $\gamma_{b,x_1}^{t_1} = a_1 \rho \lambda_{u1,b}$, $\gamma_{b,x_2}^{t_2} = \frac{a_3 \rho \lambda_{u1,b}}{a_4 \rho \lambda_{r,b} + 1}$, $\gamma_{r,y_1,2}^{t_1} = \frac{a_2 \rho \lambda_{u2,r}}{a_1 \rho \lambda_{u1,r}}$ and $\gamma_{b,y_1}^{t_2} = a_4 \rho \lambda_{r,b}$.

Hence, OP of uplink-NOMA-MEC with ideal hardware and perfect SIC under Case-2 is expressed as

$$P_O^{p,2} = P_O^{p,x_1} \times P_O^{p,x_2} \times P_{O,y_1}^{p,2}. \quad (54)$$

E. OUTAGE PERFORMANCE ANALYSIS OF UPLINK-OMA-MEC

The performance achieved by uplink-NOMA-MEC is evaluated and compared to uplink-OMA-MEC as a benchmark. We use time-division multiple access (TDMA) as the OMA. In uplink-OMA, all time slots are assigned to one user, which transmits the same information signals to BS. We analytically investigate the performance of uplink-OMA. The OP of U1 and U2 in uplink-OMA-MEC are respectively given as

$$\begin{aligned}
 P_{O,OMA}^{x_1} &= P_r(\gamma_{b,x_1}^{t_1} \leq x) \\
 &= 1 - \frac{\rho \lambda_{u1,b}}{\rho \lambda_{u1,b} + \rho \lambda_{u1,b} k_a^2 x} e^{-\frac{x}{\rho \lambda_{u1,b}}}, \quad (55)
 \end{aligned}$$

$$\begin{aligned}
 P_{O,OMA}^{x_2} &= P_r(\gamma_{b,x_2}^{t_2} \leq x) \\
 &= 1 - \frac{\rho \lambda_{u1,b}}{\rho \lambda_{u1,b} + \rho \lambda_{u1,b} k_a^2 x} e^{-\frac{x}{\rho \lambda_{u1,b}}} \quad (56)
 \end{aligned}$$

and

$$\begin{aligned}
 P_{O,OMA}^{y_1} &= P_r(\min(\gamma_{r,y_1}^{t_1}, \gamma_{b,y_1}^{t_1}) \leq y) \\
 &= 1 - \frac{\rho \lambda_{u2,r}}{\rho \lambda_{u2,r} + \rho \lambda_{u2,r} k_a^2 y} \frac{\rho \lambda_{r,b}}{\rho \lambda_{r,b} + \rho \lambda_{r,b} k_a^2 y} e^{-my}, \quad (57)
 \end{aligned}$$

where $x = 2^{4R_1} - 1$, $y = 2^{4R_2} - 1$, $m = \frac{1}{\rho \lambda_{u2,r}} + \frac{1}{\rho \lambda_{r,b}}$, $\gamma_{r,y_1}^{t_1} = \frac{\rho \lambda_{u2,r}}{\rho k_a^2 \lambda_{u2,r} + 1}$ and $\gamma_{r,y_1}^{t_1} = \frac{\rho \lambda_{r,b}}{\rho k_a^2 \lambda_{r,b} + 1}$.

Hence, OP of uplink-OMA-MEC with RHI is given as

$$P_{O,OMA} = P_{O,OMA}^{x_1} \times P_{O,OMA}^{x_2} \times P_{O,OMA}^{y_1} \quad (58)$$

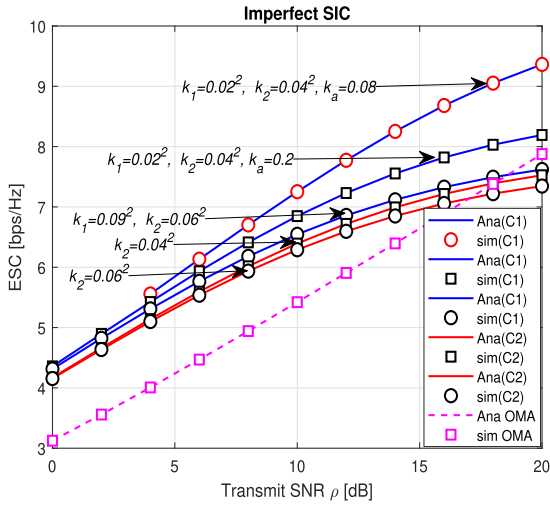


FIGURE 2. Sum capacity comparison w.r.t SNR ρ , $d_{u1,b} = 0.3$, RHI factor $k_a = 0.08$ and 0.2 , ipSIC.

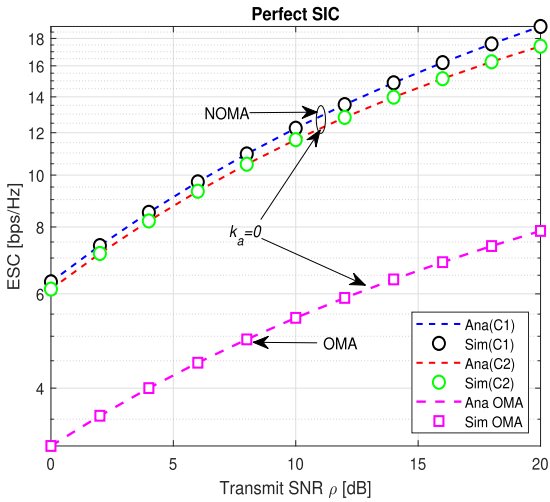


FIGURE 3. Sum capacity comparison w.r.t SNR ρ , $d_{u1,b} = 0.3$, RHI factor $k_a = 0.08$ and 0.2 , pSIC.

and With ideal hardware (i.e. $k_a = 0$), the OP is as follows

$$P_{O,OMA}^{ideal} = P_{O,OMA}^{x_1} \times P_{O,OMA}^{x_2} \times P_{O,OMA}^{y_1}, \quad (59)$$

where $P_{O,OMA}^{x_1} = P_{O,OMA}^{x_2} = 1 - e^{-\frac{x}{\rho \lambda_{u1,b}}}$ and $P_{O,OMA}^{y_1} = 1 - e^{-my}$.

IV. NUMERICAL AND SIMULATION RESULTS

In this section, we present a set of numerical parameters to validate our theoretical results by using a series of analytical measurements, symbolized by lines and a series of Monte-Carlo simulations, symbolized by markers. A fixed power allocation method [44], [45] with a fixed transmit power scheme is adopted with symmetric signal and noise powers. We consider the impact of RHI on the ESC and OP. The proposed uplink-NOMA based MEC offloading and uplink-OMA based MEC offloading compared based on their performance, in terms of ESC, OP, offloading delay

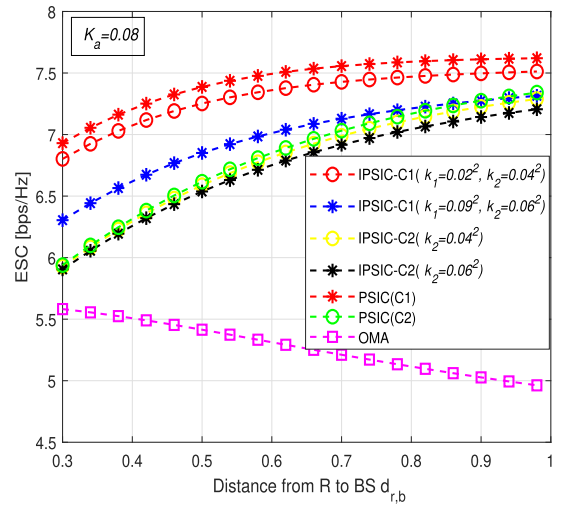


FIGURE 4. Comparison of sum capacity and normalized distance $d_{r,b} : d_{u1,b} = 0.3$.

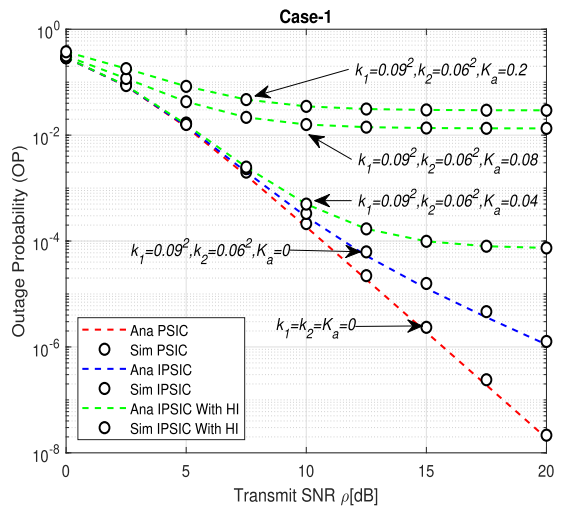


FIGURE 5. OP vs. transmit SNR ρ , Case-1, RHI factor $k_a = 0.08$ and 0.2 .

and energy consumption. This comparison is demonstrated in Figs. 2, 3 and 4. In Figs. 2 and 3, we examine two cases including normalized distances between source and sink, as well as the settings for power allocation coefficients. Case-1 (C1): $a_1 = a_3 = 0.7$, $a_2 = a_4 = 0.3$, $d_{u1,r} = 0.3$, $d_{u2,r} = d_{r,b} = 0.5$. Case-2 (C2): $a_1 = a_4 = 0.3$, $a_2 = a_3 = 0.7$, $d_{u1,r} = 0.6$, $d_{u2,r} = 0.3$, $d_{r,b} = 0.7$. Taking U2 and BS to have a normalized distance of unity between them, we have $d_{u2,b} = 1$, $d_{u1,b} = 0.3$ and path loss exponent $\chi = 3$. In Figs. 2 and 3, the capacity comparison between uplink-NOMA and uplink-OMA is shown w.r.t. transmit SNR ρ and the normalized distance $d_{r,b}$, respectively. In Case-1, we found from both figures that under perfect SIC, uplink-NOMA outperforms uplink-OMA regardless of the relay position and ρ , whereas under imperfect SIC, capacity gain depends on the relay position, ρ , k_1 and/or k_2 and impairment factor k_a . In Case-2, uplink-NOMA performs significantly better than uplink-OMA with perfect SIC and

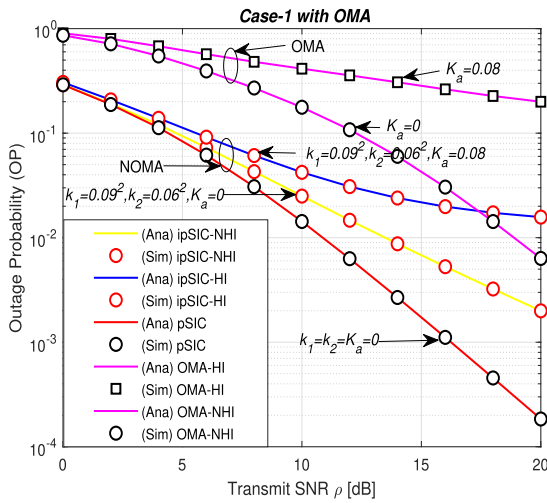


FIGURE 6. OP vs. transmit SNR ρ , Case-1 with OMA, RHI factor $k_a = 0$ and 0.08 .

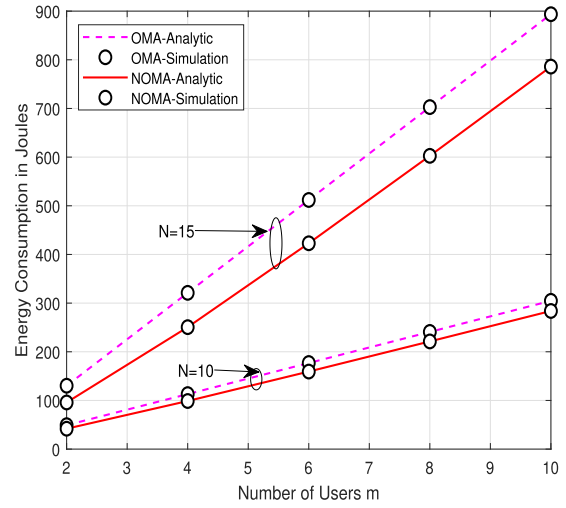


FIGURE 8. Energy consumption vs. number of users $m = 2 * M$, $N=10$ and 15 .

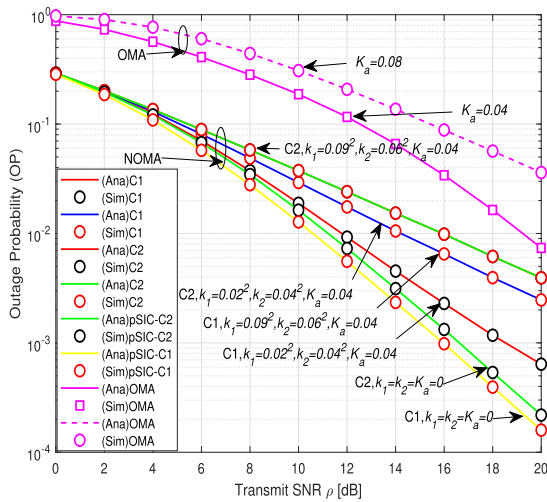


FIGURE 7. OP vs. transmit SNR ρ , all Cases with RHI factor $k_a = 0.04, 0.08$ and 0.2 .

at low to medium ρ regardless of the relay position. At high regimes, however, performance gain is largely dependent on the relay position. On the other hand, with imperfect SIC, uplink-NOMA outperforms uplink-OMA based on the relay position, ρ , k_2 and k_a . Also, it is noted that in UP-NOMA, the ESC with $k_1 = 0.02^2$, $k_2 = 0.04^2$ outperforms the ESC with $k_1 = 0.09^2$, $k_2 = 0.06^2$, indicating ESC can be much enhanced with a superior interference cancellation. From Fig. 4, it is found that ESC of uplink-OMA is maximum if the relay is almost in the middle of the range between BS and U2. Conversely, in both Case-1 and Case-2, the ESC of uplink-NOMA improves gradually until the relay reaches to a certain position towards U2 and then that ESC saturates. Figs.5 and 6 show the impact of the parameters, such as k_1 , k_2 , and k_a on the OPs for Case-1. It is evident that the system offloading OPs improves with the decrease of imperfect SIC and RHI factors. Moreover, it is pointed out that offloading OP with $k_1 = 0.09^2$, $k_2 = 0.06^2$ and $k_a = 0$ is better than the

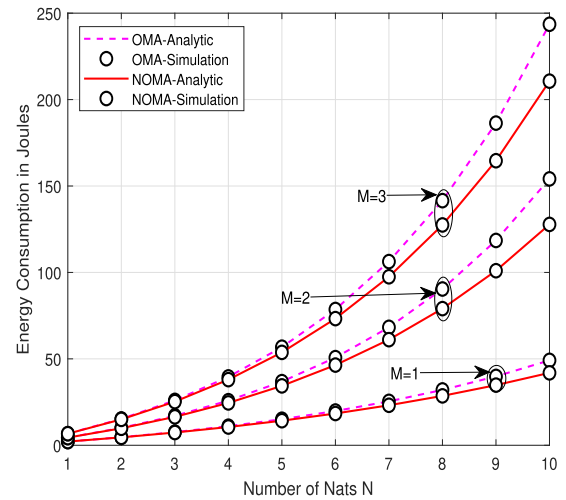


FIGURE 9. Energy consumption vs. number of Nats N , for $M=1,2$ and 3 .

offloading OP with $k_1 = 0.09^2$, $k_2 = 0.06^2$, $k_a = 0.04$ and $k_1 = 0.09^2$, $k_2 = 0.06^2$ and $k_a = 0.08$ in UP-NOMA, which indicates that the offloading OP can be improved significantly with less RHI factor. In Fig. 7, both Case-1 and Case-2 with perfect and imperfect SIC is considered for uplink-NOMA and uplink-OMA based MEC users. Uplink-NOMA outperforms uplink-OMA in terms of OPs. In Figs. 8 and 9, offloading energy consumption performance versus numbers of mobile users under the different task sizes and number of tasks is shown for NOMA-MEC offloading and OMA-MEC offloading, respectively. It is found that the offloading energy consumption increases with the increase of the number of mobile users ($m = 2, 4 \dots 10$) and with the number of computational tasks of users ($N = 10, 15$). Fig. 10 shows the offloading delay performance versus different task sizes. Delay in the system increases with the increase of number of task sizes $N-1, 2 \dots 10$, with imperfect SIC factors k_1 and k_2 and with RHI factor k_a . Additionally, it is noted

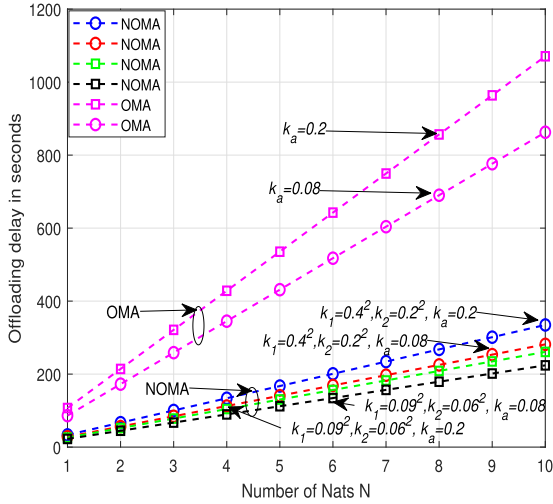


FIGURE 10. Offloading delay T vs. number of Nats N with $k_a = 0.08$ and 0.2 .

that MEC system offloading delay with $k_1 = 0.09^2$, $k_2 = 0.06^2$ and $k_a = 0.08$ is better than the offloading delay with $k_1 = 0.4^2$, $k_2 = 0.2^2$ and $k_a = 0.2$ which suggests that smaller RHI factors and greater interference cancellation can greatly reduce offloading latency. Offloading tasks in OMA require the far user to be in a specific time slot, while in NOMA-MEC, it is the near user who can enter the slot to begin its offloading tasks. In contrast to OMA-MEC, NOMA-MEC does not require an additional time slot for the near user, reducing the system's offloading delay. In this sense, NOMA-MEC requires less energy to run when a similar number of computational tasks is offloaded to it as OMA-MEC.

V. CONCLUSION

In this paper, we proposed an edge commuting-aware NOMA technique to reduce MEC users' energy consumption and latency by leveraging the benefits of uplink NOMA. The use of cooperative communications in the form of relaying can be incorporated into the wireless-powered MEC systems, which can effectively reduce the transmitted energy [46]. Additionally, CDRT-based NOMA-MEC system offloading performance has been examined when the system is operating in the presence of RHI and imperfect SIC. The main benefit of CDRT in NOMA is that the sum-capacity scaling as SNR increases, but it is half for NOMA in non-CDRT [25], [47]. The exact expressions of offloading OP, ESC, offloading delay, and energy consumption for the paired users were derived in detail and compared with the uplink OMA-based MEC system. The analytical and simulation results show that NOMA-MEC outperforms OMA-MEC in offloading OP, ESC, offloading delay, and energy consumption under a fixed power allocation scheme. Based on residual interference levels, SIC factors, relay positions, and transmit SNR, uplink-NOMA yields higher capacity gains than uplink-OMA. It becomes more likely for NOMA-MEC to experience offloading outages when RHI and imperfect SIC parameters

increase. In addition, the impact of changing the number of offloading users or tasks on users' energy consumption and latency has also been explored. The outcome of this paper indicates that uplink-NOMA-based MEC could be an effective strategy for enhancing system capacity, improving the use of quality of service by far users, and reducing the latency and energy consumption of users in next-generation wireless networks. It is an important topic to examine how imperfect CSI affects NOMA-MEC is a crucial area for future research. Additionally, It is possible to improve the performance of NOMA over OMA by scheduling more users in one NOMA group, instead of only two users as in this paper. and it can be an important topic for future research. However, the implementation complexity increases as more users are included in the same group. In light of this, it may be more practical to divide the users into smaller groups, and the users within one group are served via NOMA. The application of advanced signal processing techniques to user clustering, an area that shows promise for future research, includes game theory and matching theory [48], [49]. Research into integrating and utilizing NOMA in MEC is still at an early stage, specifically to edge user allocation.

APPENDIX A

PROOF OF EC OF NEAR USER (U1)

$$\begin{aligned} \tilde{R}_c^{u1} &= E \{R_{x1}^{t1}\} + E \{R_{x2}^{t2}\} \\ &= \underbrace{\frac{1}{2} \int_0^\infty \log_2(1+z_1) f_{Z_1}(z_1) dz_1}_{I_1} + \underbrace{\frac{1}{2} \int_0^\infty \log_2(1+z_2) f_{Z_2}(z_2) dz_2}_{I_2} \end{aligned} \quad (60)$$

$$\begin{aligned} I_1 &= \frac{1}{2} \frac{1}{\ln 2} \int_0^\infty \frac{1 - F_{Z_1}(z_1)}{1+z_1} dz_1 \\ &= \frac{\log_2 e}{2} \int_0^\infty \frac{e^{-\frac{z_1}{a_1 \rho \lambda_{u1,b}}}}{1+z_1} \frac{1}{1+k_a^2 z_1} dz_1 \\ &= \frac{\log_2 e}{2} \int_0^\infty \frac{(1+z_1)^{-1}}{1+k_a^2 z_1} \left\{ \frac{1+k_a^2 z_1}{1-k_a^2} - \frac{1+k_a^2(1+z_1)}{1-k_a^2} \right\} \\ &\quad \times e^{-\frac{z_1}{a_1 \rho \lambda_{u1,b}}} dz_1 \\ &= \frac{\log_2 e}{2} \frac{1}{1-k_a^2} \left\{ \int_0^\infty (1+z_1)^{-1} e^{-\frac{z_1}{a_1 \rho \lambda_{u1,b}}} dz_1 \right. \\ &\quad \left. - \int_0^\infty \frac{k_a^2}{1+k_a^2 z_1} e^{-\frac{z_1}{a_1 \rho \lambda_{u1,b}}} dz_1 \right\} \\ &= \frac{\log_2 e}{2} \frac{1}{1-k_a^2} \left[\left\{ -e^{-\frac{1}{a_1 \rho \lambda_{u1,b}}} Ei\left(-\frac{1}{a_1 \rho \lambda_{u1,b}}\right) \right\} \right. \\ &\quad \left. + \left\{ e^{a_1 \rho k_a^2 \lambda_{u1,b}} Ei\left(-\frac{1}{a_1 \rho k_a^2 \lambda_{u1,b}}\right) \right\} \right] \end{aligned} \quad (61)$$

and following the similar steps to evaluate (61), I_2 can be evaluated as

$$\begin{aligned} I_2 &= \frac{1}{2} \int_0^\infty \log_2(1+z_2) f_{Z_2}(z_2) dz_2 \\ &= \frac{\log_2 e}{2} \frac{k}{k-1} \left[\frac{1}{l-1} \left\{ -e^{m_1} Ei(-m_1) + e^{l m_1} Ei(-l m_1) \right\} \right. \\ &\quad \left. + \frac{l}{l-k} \left\{ -e^{k m_1} Ei(-k m_1) + e^{l m_1} Ei(-l m_1) \right\} \right]. \end{aligned}$$

APPENDIX B
PROOF OF EC OF FAR USER (U2) UNDER CASE-1

$$\begin{aligned} \tilde{R}_{c,1}^{u2} &= \frac{1}{2} \int_0^\infty \log_2(1+v) f_V(v) dv \\ &= \frac{\log_2 e}{2} \int_0^\infty \frac{p(1+v)^{-1}}{p+v} \left\{ \frac{p+v}{p-1} - \frac{1+v}{p-1} \right\} \frac{q}{q+v} \\ &\quad \times \frac{s}{s+v} \times \frac{t}{t+v} \times e^{-m_2 v} dv \\ &= \frac{\log_2 e}{2} \frac{p}{p-1} \int_0^\infty \left\{ \frac{q(1+v)^{-1}}{q+v} - \frac{q(p+v)^{-1}}{q+v} \right\} \\ &\quad \times \frac{s}{s+v} \times \frac{t}{t+v} e^{-m_2 v} dv \\ &= \left[\underbrace{g \frac{q}{q-1} \int_0^\infty \left\{ \frac{(1+v)^{-1}}{-(q+v)^{-1}} \right\} \frac{s}{s+v} \times \frac{t}{t+v} \times e^{-m_2 v} dv}_{I_3} \right. \\ &\quad \left. - \underbrace{g \frac{q}{q-p} \int_0^\infty \left\{ \frac{(p+v)^{-1}}{-(q+v)^{-1}} \right\} \frac{s}{s+v} \times \frac{t}{t+v} \times e^{-m_2 v} dv}_{I_4} \right] \end{aligned} \tag{62}$$

where

$$\begin{aligned} I_3 &= g \frac{q}{q-1} \int_0^\infty \left[\frac{(1+v)^{-1}}{-(q+v)^{-1}} \frac{s}{s+v} \left\{ \frac{s+v}{s-1} - \frac{1+v}{s-1} \right\} \right] \frac{t}{t+v} \\ &\quad \times e^{-m_2 v} dv \\ &= g_1 \int_0^\infty \left[\frac{t}{t+v} (1+v)^{-1} \left\{ \frac{t+v}{t-1} - \frac{1+v}{t-1} \right\} \right. \\ &\quad \left. - \frac{t}{t+v} (s+v)^{-1} \left\{ \frac{t+v}{t-s} - \frac{s+v}{t-s} \right\} \right] e^{-m_2 v} dv \\ &\quad - g_2 \int_0^\infty \left[\frac{t}{t+v} (q+v)^{-1} \left\{ \frac{t+v}{t-q} - \frac{q+v}{t-q} \right\} \right. \\ &\quad \left. - \frac{t}{t+v} (s+v)^{-1} \left\{ \frac{t+v}{t-s} - \frac{s+v}{t-s} \right\} \right] e^{-m_2 v} dv \\ &= g_1 \frac{t}{t-1} \int_0^\infty \left\{ (1+v)^{-1} - (t+v)^{-1} \right\} e^{-m_2 v} dv \\ &\quad - g_1 \frac{t}{t-s} \int_0^\infty \left\{ (s+v)^{-1} - (t+v)^{-1} \right\} e^{-m_2 v} dv \\ &\quad - g_2 \frac{t}{t-q} \int_0^\infty \left\{ (q+v)^{-1} - (t+v)^{-1} \right\} e^{-m_2 v} dv \\ &\quad + g_2 \frac{t}{t-s} \int_0^\infty \left\{ (s+v)^{-1} - (t+v)^{-1} \right\} e^{-m_2 v} dv. \end{aligned}$$

Using [43, eq.(3.352.4)], we have

$$\begin{aligned} I_3 &= g_1 \frac{t}{t-1} \left\{ -e^{m_2} Ei(-m_2) + e^{tm_2} Ei(-tm_2) \right\} \\ &\quad - g_1 \frac{t}{t-s} \left\{ -e^{sm_2} Ei(-sm_2) + e^{tm_2} Ei(-tm_2) \right\} \\ &\quad - g_2 \frac{t}{t-q} \left\{ -e^{qm_2} Ei(-qm_2) + e^{tm_2} Ei(-tm_2) \right\} \\ &\quad + g_2 \frac{t}{t-s} \left\{ -e^{sm_2} Ei(-sm_2) + e^{tm_2} Ei(-tm_2) \right\} \end{aligned} \tag{63}$$

Following the similar steps to evaluate (63), I_4 can be evaluated as

$$\begin{aligned} I_4 &= g \frac{q}{q-p} \int_0^\infty \left\{ (p+v)^{-1} \frac{s}{s+v} - (q+v)^{-1} \frac{s}{s+v} \right\} \frac{t}{t+v} e^{-m_2 v} dv \\ &= g_3 \frac{t}{t-p} \int_0^\infty \left\{ (p+v)^{-1} - (t+v)^{-1} \right\} e^{-m_2 v} dv \end{aligned}$$

$$\begin{aligned} &-g_3 \frac{t}{t-s} \int_0^\infty \left\{ (s+v)^{-1} - (t+v)^{-1} \right\} e^{-m_2 v} dv \\ &-g_4 \frac{t}{t-q} \int_0^\infty \left\{ (q+v)^{-1} - (t+v)^{-1} \right\} e^{-m_2 v} dv \\ &+g_4 \frac{t}{t-s} \int_0^\infty \left\{ (s+v)^{-1} - (t+v)^{-1} \right\} e^{-m_2 v} dv \end{aligned}$$

Now using [43, eq.(3.352.4)], we have

$$\begin{aligned} I_4 &= g_3 \frac{t}{t-p} \left\{ -e^{pm_2} Ei(-pm_2) + e^{tm_2} Ei(-tm_2) \right\} \\ &\quad - g_3 \frac{t}{t-s} \left\{ -e^{sm_2} Ei(-sm_2) + e^{tm_2} Ei(-tm_2) \right\} \\ &\quad - g_4 \frac{t}{t-q} \left\{ -e^{qm_2} Ei(-qm_2) + e^{tm_2} Ei(-tm_2) \right\} \\ &\quad + g_4 \frac{t}{t-s} \left\{ -e^{sm_2} Ei(-sm_2) + e^{tm_2} Ei(-tm_2) \right\} \end{aligned} \tag{64}$$

REFERENCES

- [1] E. Bastug, M. Bennis, M. Medard, and M. Debbah, "Toward interconnected virtual reality: Opportunities, challenges, and enablers," *IEEE Commun. Mag.*, vol. 55, no. 6, pp. 110–117, Jun. 2017.
- [2] M. Hua, H. Tian, W. Ni, and S. Fan, "Energy efficient task offloading in NOMA-based mobile edge computing system," in *Proc. IEEE PIMRC*, Sep. 2019, pp. 1–7.
- [3] Z. Ding, P. Fan, and H. V. Poor, "Impact of non-orthogonal multiple access on the offloading of mobile edge computing," *IEEE Trans. Commun.*, vol. 67, no. 1, pp. 375–390, Jan. 2019.
- [4] A. Kiani and N. Ansari, "Edge computing aware NOMA for 5G networks," *IEEE Internet Things J.*, vol. 5, no. 2, pp. 1299–1306, Apr. 2018.
- [5] Y. Pan, M. Chen, Z. Yang, N. Huang, and M. Shikh-Bahaei, "Energy-efficient NOMA-based mobile edge computing offloading," *IEEE Commun. Lett.*, vol. 23, no. 2, pp. 310–313, Feb. 2019.
- [6] Z. Ding, D. Xu, R. Schober, and H. V. Poor, "Hybrid NOMA offloading in multi-user MEC networks," *IEEE Trans. Wireless Commun.*, vol. 21, no. 7, pp. 5377–5391, Jul. 2022.
- [7] Y. Ye, R. Q. Hu, G. Lu, and L. Shi, "Enhance latency-constrained computation in MEC networks using uplink NOMA," *IEEE Trans. Commun.*, vol. 68, no. 4, pp. 2409–2425, Apr. 2020.
- [8] L. Zeng, W. Wen, and C. Dong, "QoS-aware task offloading with NOMA-based resource allocation for mobile edge computing," in *Proc. IEEE WCNC*, Apr. 2022, pp. 1242–1247.
- [9] Z. Ding, Y. Liu, J. Choi, Q. Sun, M. Elkashlan, I. Chih-Lin, and H. V. Poor, "Application of non-orthogonal multiple access in LTE and 5G networks," *IEEE Commun. Mag.*, vol. 55, no. 2, pp. 185–191, Feb. 2017.
- [10] A. F. M. S. Shah, A. N. Qasim, M. A. Karabulut, H. Ilhan, and M. B. Islam, "Survey and performance evaluation of multiple access schemes for next-generation wireless communication systems," *IEEE Access*, vol. 9, pp. 113428–113442, 2021.
- [11] Z. Yang, Z. Ding, P. Fan, and N. Al-Dhahir, "A general power allocation scheme to guarantee quality of service in downlink and uplink NOMA systems," *IEEE Trans. Wireless Commun.*, vol. 15, no. 11, pp. 7244–7257, Nov. 2016.
- [12] S. M. R. Islam, N. Avazov, O. A. Dobre, and K.-S. Kwak, "Power-domain non-orthogonal multiple access (NOMA) in 5G systems: Potentials and challenges," *IEEE Commun. Surveys Tuts.*, vol. 19, no. 2, pp. 721–742, 2nd Quart., 2017.
- [13] E. A. Hassan, Z. Mumtaz, and Z. Ali, "A survey on power domain non-orthogonal multiple access (NOMA) based communication system," *IEEE Commun. Surveys Tuts.*, vol. 19, pp. 721–742, 2016.
- [14] J. Du, W. Liu, G. Lu, J. Jiang, D. Zhai, F. R. Yu, and Z. Ding, "When mobile-edge computing (MEC) meets nonorthogonal multiple access (NOMA) for the Internet of Things (IoT): System design and optimization," *IEEE Internet Things J.*, vol. 8, no. 10, pp. 7849–7862, May 2021.
- [15] Y. Huang, Y. Liu, and F. Chen, "NOMA-aided mobile edge computing via user cooperation," *IEEE Trans. Commun.*, vol. 68, no. 4, pp. 2221–2235, Apr. 2020.

- [16] Y. Wu, K. Ni, C. Zhang, L. P. Qian, and D. H. K. Tsang, "NOMA-assisted multi-access mobile edge computing: A joint optimization of computation offloading and time allocation," *IEEE Trans. Veh. Technol.*, vol. 67, no. 12, pp. 12244–12258, Dec. 2018.
- [17] M. Sheng, Y. Dai, J. Liu, N. Cheng, X. Shen, and Q. Yang, "Delay-aware computation offloading in NOMA MEC under differentiated uploading delay," *IEEE Trans. Wireless Commun.*, vol. 19, no. 4, pp. 2813–2826, Apr. 2020.
- [18] Z. Yang, C. Pan, J. Hou, and M. Shikh-Bahaei, "Efficient resource allocation for mobile-edge computing networks with NOMA: Completion time and energy minimization," *IEEE Trans. Commun.*, vol. 67, no. 11, pp. 7771–7784, Nov. 2019.
- [19] J. Zhu, J. Wang, Y. Huang, F. Fang, K. Navaie, and Z. Ding, "Resource allocation for hybrid NOMA MEC offloading," *IEEE Trans. Wireless Commun.*, vol. 19, no. 7, pp. 4964–4977, Jul. 2020.
- [20] K. Zheng, G. Jiang, X. Liu, K. Chi, X. Yao, and J. Liu, "DRL-based offloading for computation delay minimization in wireless-powered multi-access edge computing," *IEEE Trans. Commun.*, vol. 71, no. 3, pp. 1755–1770, Mar. 2023.
- [21] X. Liu, B. Xu, K. Zheng, and H. Zheng, "Throughput maximization of wireless-powered communication network with mobile access points," *IEEE Trans. Wireless Commun.*, vol. 22, no. 7, pp. 4401–4415, Jul. 2022.
- [22] W. Wu, F. Zhou, R. Q. Hu, and B. Wang, "Energy-efficient resource allocation for secure NOMA-enabled mobile edge computing networks," *IEEE Trans. Commun.*, vol. 68, no. 1, pp. 493–505, Jan. 2020.
- [23] S. M. R. Islam, M. Zeng, O. A. Dobre, and K.-S. Kwak, "Resource allocation for downlink NOMA systems: Key techniques and open issues," *IEEE Wireless Commun.*, vol. 25, no. 2, pp. 40–47, Apr. 2018.
- [24] L. Dai, B. Wang, Z. Ding, Z. Wang, S. Chen, and L. Hanzo, "A survey of non-orthogonal multiple access for 5G," *IEEE Commun. Surveys Tuts.*, vol. 20, no. 3, pp. 2294–2323, 3rd Quart., 2018.
- [25] J.-B. Kim and I.-H. Lee, "Non-orthogonal multiple access in coordinated direct and relay transmission," *IEEE Commun. Lett.*, vol. 19, no. 11, pp. 2037–2040, Nov. 2015.
- [26] A. Jee, K. Agrawal, and S. Prakriya, "A coordinated direct AF/DF relay-aided NOMA framework for low outage," *IEEE Trans. Commun.*, vol. 70, no. 3, pp. 1559–1579, Mar. 2022.
- [27] Md. F. Kader and S. Y. Shin, "Coordinated direct and relay transmission using uplink NOMA," *IEEE Wireless Commun. Lett.*, vol. 7, no. 3, pp. 400–403, Jun. 2018.
- [28] S. K. Sa and A. K. Mishra, "An uplink cooperative NOMA based on CDRT with hardware impairments and imperfect CSI," *IEEE Syst. J.*, vol. 17, no. 4, pp. 5695–5705, Dec. 2023.
- [29] T. Schenk, *RF Imperfections in High-Rate Wireless Systems: Impact and Digital Compensation*. New York, NY, USA: Springer, 2008.
- [30] X. Li, Q. Wang, M. Liu, J. Li, H. Peng, Md. J. Piran, and L. Li, "Cooperative wireless-powered NOMA relaying for B5G IoT networks with hardware impairments and channel estimation errors," *IEEE Internet Things J.*, vol. 8, no. 7, pp. 5453–5467, Apr. 2021.
- [31] T. Mazhar, M. A. Malik, S. A. H. Mohsan, Y. Li, I. Haq, S. Ghorashi, F. K. Karim, and S. M. Mostafa, "Quality of service (QoS) performance analysis in a traffic engineering model for next-generation wireless sensor networks," *Symmetry*, vol. 15, no. 2, p. 513, Feb. 2023.
- [32] C. She, R. Dong, Z. Gu, Z. Hou, Y. Li, W. Hardjawana, C. Yang, L. Song, and B. Vucetic, "Deep learning for ultra-reliable and low-latency communications in 6G networks," *IEEE Netw.*, vol. 34, no. 5, pp. 219–225, Sep. 2020.
- [33] X. Li, J. Li, Y. Liu, Z. Ding, and A. Nallanathan, "Residual transceiver hardware impairments on cooperative NOMA networks," *IEEE Trans. Wireless Commun.*, vol. 19, no. 1, pp. 680–695, Jan. 2020.
- [34] N. P. Le and K. N. Le, "Uplink NOMA short-packet communications with residual hardware impairments and channel estimation errors," *IEEE Trans. Veh. Technol.*, vol. 71, no. 4, pp. 4057–4072, Apr. 2022.
- [35] M.-S. Van Nguyen, D.-T. Do, Z. D. Zaharis, C. X. Mavromoustakis, G. Matorakis, and E. Pallis, "Enabling full-duplex in MEC networks using uplink NOMA in presence of hardware impairments," *Wireless Pers. Commun.*, vol. 120, no. 3, pp. 1945–1973, Oct. 2021.
- [36] B. Li, W. Wu, W. Zhao, and H. Zhang, "Security enhancement with a hybrid cooperative NOMA scheme for MEC system," *IEEE Trans. Veh. Technol.*, vol. 70, no. 3, pp. 2635–2648, Mar. 2021.
- [37] M. S. Ali, H. Tabassum, and E. Hossain, "Dynamic user clustering and power allocation for uplink and downlink non-orthogonal multiple access (NOMA) systems," *IEEE Access*, vol. 4, pp. 6325–6343, 2016.
- [38] Y. Xu, G. Wang, B. Li, and S. Jia, "Performance of D2D aided uplink coordinated direct and relay transmission using NOMA," *IEEE Access*, vol. 7, pp. 151090–151102, 2019.
- [39] E. Bjornson, M. Matthaiou, and M. Debbah, "A new look at dual-hop relaying: Performance limits with hardware impairments," *IEEE Trans. Commun.*, vol. 61, no. 11, pp. 4512–4525, Nov. 2013.
- [40] A. K. Mishra and P. Singh, "Performance analysis of opportunistic transmission in downlink cellular DF relay network with channel estimation error and RF impairments," *IEEE Trans. Veh. Technol.*, vol. 67, no. 9, pp. 9021–9026, Sep. 2018.
- [41] C. Zhong and Z. Zhang, "Non-orthogonal multiple access with cooperative full-duplex relaying," *IEEE Commun. Lett.*, vol. 20, no. 12, pp. 2478–2481, Dec. 2016.
- [42] X. Li, M. Zhao, M. Zeng, S. Mumtaz, V. G. Menon, Z. Ding, and O. A. Dobre, "Hardware impaired ambient backscatter NOMA systems: Reliability and security," *IEEE Trans. Commun.*, vol. 69, no. 4, pp. 2723–2736, Apr. 2021.
- [43] I. S. Gradshteyn and I. Ryzhik, *Table of Integrals, Series, and Products*, 7th ed., New York, NY, USA: Academic, 2007.
- [44] Z. Ding, H. Dai, and H. V. Poor, "Relay selection for cooperative NOMA," *IEEE Wireless Commun. Lett.*, vol. 5, no. 4, pp. 416–419, Aug. 2016.
- [45] Z. Wei, L. Dai, D. W. K. Ng, and J. Yuan, "Performance analysis of a hybrid downlink-uplink cooperative NOMA scheme," in *Proc. IEEE VTC Spring*, Jun. 2017, pp. 1–7.
- [46] X. Hu, K.-K. Wong, and K. Yang, "Wireless powered cooperation-assisted mobile edge computing," *IEEE Trans. Wireless Commun.*, vol. 17, no. 4, pp. 2375–2388, Apr. 2018.
- [47] C. D. T. Thai and P. Popovski, "Coordinated direct and relay transmission with interference cancellation in wireless systems," *IEEE Commun. Lett.*, vol. 15, no. 4, pp. 416–418, Apr. 2011.
- [48] B. Di, L. Song, and Y. Li, "Sub-channel assignment, power allocation, and user scheduling for non-orthogonal multiple access networks," *IEEE Trans. Wireless Commun.*, vol. 15, no. 11, pp. 7686–7698, Nov. 2016.
- [49] W. Liang, Z. Ding, Y. Li, and L. Song, "User pairing for downlink non-orthogonal multiple access networks using matching algorithm," *IEEE Trans. Commun.*, vol. 65, no. 12, pp. 5319–5332, Dec. 2017.



SUDHIR KUMAR SA received the M.Tech. degree in information and communication technology (ICT) from the Dhirubhai Ambani Institute of Information and Communication Technology (DA-IICT), Gandhinagar, India, in 2009. He is currently pursuing the Ph.D. degree with the School of Electronics Engineering, Vellore Institute of Technology (VIT), AP University, Andhra Pradesh, India. His research interests include cooperative communications, nonorthogonal multiple access, delay and security-aware MEC networks, relaying strategies over fading channels, energy harvesting, and non-orthogonal multiple access.



ANOOP KUMAR MISHRA (Member, IEEE) received the B.E. degree in electronics and communication engineering from Rajiv Gandhi Pradyogiki Vishwavidyalaya, Bhopal, India, in 2010, and the Ph.D. degree in electronics and communication engineering from the National Institute of Technology, Rourkela, India, in 2018. Currently, he is an Associate Professor with the School of Electronics Engineering, Vellore Institute of Technology, Amaravati, Andhra Pradesh, India. His research interests include cooperative communications, non-orthogonal multiple access, delay and security-aware MEC networks, relaying strategies over fading channels, and energy harvesting. He was a recipient of Lalita and Ravindra Nath Foundation Award, in 2017.

• • •